Kinetic and Mechanistic Studies of Penicillin-Binding Protein 2x from *Streptococcus pneumoniae*

Beth Thomas, Yi Wang, and Ross L. Stein*

Department of Chemical Enzymology, DuPont Pharmaceuticals Company, Wilmington, Delaware 19880

Received June 29, 2001; Revised Manuscript Received September 10, 2001

ABSTRACT: High molecular weight penicillin-binding proteins (PBPs) are bifunctional enzymes that build bacterial cell walls from the glycopeptide lipid II [GlcNAc-MurNAc(L-Ala-γ-D-Glu-L-Lys-D-Ala-D-Ala)-pyrophosphate-undecaprenol] by a process involving disaccharide polymerization and peptide cross-linking. The latter reaction involves acyl-transfer chemistry in which the penultimate (D)Ala first acylates the active-site serine, with release of the terminal (D)Ala, and is then transferred to the ϵ-amine of a Lys on a neighboring pentapeptide chain. These enzymes also catalyze hydrolysis of specific thioester substrates and acylation by β-lactam antibiotics. In this paper, we explore these latter two reactions and report mechanistic experiments on the reaction of *Streptococcus pneumoniae* PBP 2x with *N*-benzoyl-(D)Ala-thioacetic acid [Bz-(D)Ala-^{S}Gly] and penicillin G. For these experiments, we used PBP 2x*, a soluble form of PBP 2x in which the transmembrane domain was deleted. The following results are significant: (1) pH dependencies for acylation of PBP 2x* by penicillin G and Bz-(D)Ala-^{S}Gly are identical, suggesting that the same ionizable residues are involved in both reactions and that these residues play the same catalytic role in the two processes. On the basis of these results, we propose a mechanistic model that is also consistent with recently published structural data [Gordon, E., et al. (2000) *J. Mol. Biol. 299*, 477−485]. (2) Pre-steady-state experiments for the PBP 2x*-catalyzed hydrolysis of Bz-(D)Ala-^{S}Gly at pH 6.5 indicate that k_c is principally rate-limited by acylation with some contribution from deacylation. The contribution of these steps to rate limitation is pH-dependent, with acylation entirely rate-limiting at pH values less than 5.5 and deacylation principally rate-limiting above pH 8.5. (3) Results of solvent isotope effect and proton inventory experiments for acylation suggest a complex process that is at least partially rate-limited by chemistry with some involvement of changes in solvation and/or enzyme conformation. (4) Analysis of activation parameters suggests that during the acylation of PBP 2x* by penicillin G the inherent chemical stability of penicillin's amide bond, as manifested in the enthalpy of activation, is offset by a favorable entropy term that reflects penicillin's rotationally constrained bicyclic system, which presumably allows a less energetically demanding entry into the transition state for acylation.

Penicillin-binding proteins comprise a large family of bacterial enzymes that catalyze essential reactions in the biosynthesis of cell wall peptidoglycan from the glycopeptide precursor lipid II (*1*−*3*). Two of these reactions are illustrated in Scheme 1: transglycosylation, which polymerizes the disaccharides of lipid II monomeric units into the backbone of the peptidoglycan, and transpeptidation, which cross-links this backbone into a tight weblike structure. These two reactions are catalyzed either by low molecular weight, monofunctional PBPs[1] or by certain high molecular weight PBPs that contain two independent catalytic domains for these activities.

PBPs derive their name from their facile interaction with penicillin and other β-lactam antibiotics (*1*−*3*). The transpeptidase domains of PBPs contain an active-site serine that nucleophilically attacks the carbonyl carbon of the β-lactam ring of these antibiotics to form an acyl-enzyme that is stable and catalytically inactive. The chemistry of the transpeptidase active site has led to the development of structurally simple, thioester substrates, such as Bz-(D)Ala-^{S}Gly, which mimic the (D)Ala−(D)Ala bond that PBPs recognize in their natural substrate. Hydrolysis of Bz-(D)Ala-^{S}Gly is thought to proceed according to the general mechanism of Scheme 2 involving the intermediacy of an acyl-enzyme. The steady-state rate expressions for this mechanism are

$$\frac{k_c}{K_m} = \frac{k_{acyl}}{K_s} \quad (1)$$

$$k_c = \frac{k_{acyl}k_{deacyl}}{k_{acyl} + k_{deacyl}} \quad (2)$$

$$K_m = K_s\frac{k_{deacyl}}{k_{acyl} + k_{deacyl}} \quad (3)$$

Unlike the acyl-enzyme formed during interaction of β-lac-

* To whom correspondence should be addressed at the Laboratory for Drug Discovery in Neurodegeneration, Harvard Center for Neurodegeneration and Repair, 65 Landsdowne St., Fourth Floor, Cambridge, MA 02139. Phone 617-768-8651; e-mail rstein@rics.bwh.harvard.edu.

[1] Abbreviations: PBP, penicillin-binding protein; Bz, *N*-benzoyl; Bz-(D)Ala-^{S}Gly, thioester analogue of Bz-(D)Ala-Gly; MALDI-TOF, matrix-assisted laser desorption ionization time-of-flight; PCR, polymerase chain reaction; PBS, phosphate-buffered saline; DTNB, 5,5′-dithiobis(2-nitrobenzoic acid); DMSO, dimethyl sulfoxide; SDS−PAGE, sodium dodecyl sulfate−polyacrylamide gel electrophoresis; MES, 2-(*N*-morpholino)ethanesulfonic acid; CHES, 2-(cyclohexylamino)-1-propanesulfonic acid.

10.1021/bi011368r CCC: $20.00
Published on Web 12/01/2001

Scheme 1: Polymerization of Lipid II in the Biosynthesis of Peptidoglycan

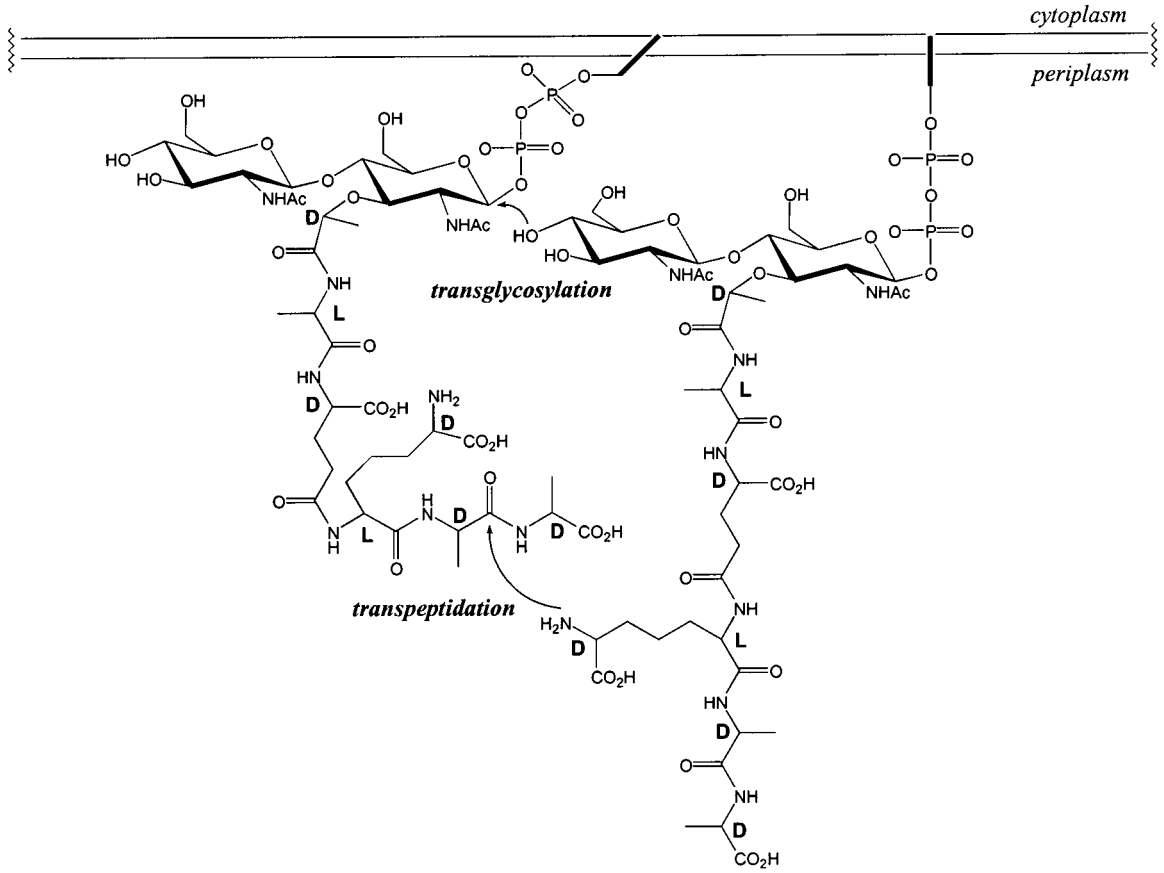

Scheme 2: Acyl-Enzyme Mechanism for the PBP 2x*-Catalyzed Hydrolysis of Bz-(d)Ala-^{S}Gly

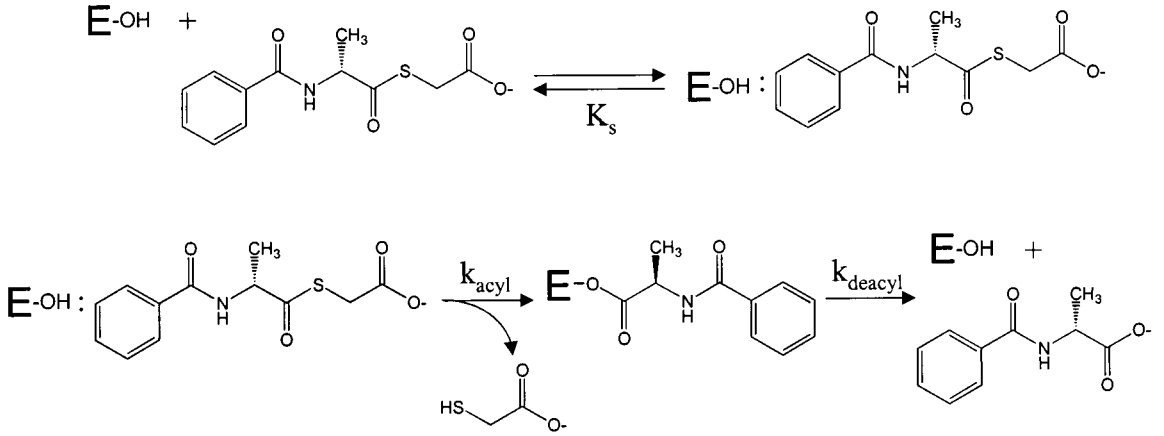

tam antibiotics with PBPs, this intermediate is reactive toward water and, thus, allows ready hydrolytic turnover of Bz-(D)Ala-^{S}Gly and similar substrates.

As part of a research program to discover novel antibacterial agents, we have initiated investigations of the catalytic mechanism of PBP 2x, an enzyme that is essential for the viability of the pathogenic organism *Streptococcus pneumoniae* (*4*). This enzyme is of interest to drug discovery not only because of its role in human disease but also because its crystal structure has been solved (*5*,*6*). Despite the clear importance of this enzyme and the possibility of structure-based inhibitor design that is promised by the advent of the X-ray structure of PBP 2x, understanding of its mechanisms of catalysis and inactivation is still at a primitive stage (*7*). In this paper, we report some of our initial mechanistic studies of PBP 2x*, the truncated and soluble form of the enzyme that was used in the X-ray crystallographic studies (*8*). Specifically in our studies, we set out to understand the mechanism of hydrolysis of Bz-(D)Ala-^{S}Gly and conducted experiments in which we probed three mechanistic areas: (i) pH dependencies of steady-state rate parameters, (ii) identity of rate-limiting steps, and (iii) structural features of rate-limiting transition states. In addition, we explored mechanistic similarities between acylation of PBP 2x* by Bz-(D)Ala-^{S}Gly and by penicillin G.

MATERIALS AND METHODS

General. Buffer salts, deuterium oxide, and penicillin G were from Sigma Chemical Co. Bz-(D)Ala-^{S}Gly was purchased from Absolute Science (Cambridge, MA). Chemical

purity was >98% as judged by HPLC analysis. Structure was confirmed by mass spectral analysis (MALDI-TOF DE; within 0.1% of exact molecular weight).

Cloning, Expression, and Purification of PBP 2x.* The gene encoding PBP 2x* (Δ1−50, transmembrane domain deleted) was amplified from the *Streptococcus pneumonia* genomic library (American Type Culture Collection) by PCR. The DNA sequences of the sense primers is ACATATGGGCACTCGCTTTGGAACAGATTTAG. An *Nde*I site was included at the 5′-end of the sense primer and a *Bam*HI site was included at the 5′-end of the antisense primer. The PCR product was subsequently inserted into a pET-21a expression vector (Novagen) between the *Nde*I and *Bam*HI sites, resulting in the introduction of a hexaHis tag at the C-terminus of the expressed protein. *Escherichia coli* strains BL21 and DE3 were transformed with this vector and show high levels of expression of PBP 2x* (∼30 mg/L). The protein was purified according to standard Ni^{2+}-column procedures. Briefly, cells were resuspended in loading buffer (50 mM NaP_i and 100 mM NaCl, pH 8.0) and disrupted in a French press. After brief centrifugation to remove cell debris, the supernatant was loaded onto a Ni^{2+}−agarose column and the column wash sequentially with 5× and 3× bed volumes of loading buffer and loading buffer with 25 mM imidazole. Finally, His-tagged PBP 2x* is specifically eluted with a wash with loading buffer containing 500 mM imidazole. After dialysis against PBS, PBP 2x* was concentrated and stored in 50% glycerol at −20 °C ($[PBP\ 2x^*]_{stock} = 9\ \mu M$).

Kinetic Methods: (A) Measurement of Steady-State Rates for PBP 2x-Catalyzed Thioester Hydrolysis. Depending on the reaction pH, we used one of two methods to measure rates of thioester hydrolysis. At pH values of 6.0 and above, we used a coupled assay in which the thiol product of thioester hydrolysis is allowed to react with DTNB that is added to the assay buffer. This coupling reaction produces a mixed disulfide and the chromophoric 2-nitro-4-carboxybenzoic acid ($\Delta\epsilon_{412} = 13\,000$). At pH values below 6.0, where reaction of thiol with DTNB is prohibitively slow, we monitored the decrease in absorbance at 250 nm that accompanies thioester hydrolysis ($\Delta\epsilon_{250} = -2200$).

In our standard assay at pH 6.5, 4 μL of a 50 mM solution of Bz-(D)-Ala-^{S}Gly in DMSO and 2 μL of a 500 mM solution of DTNB in DMSO are added to 2.00 mL of assay buffer (50 mM MES and 500 mM KCl, pH 6.5) in a 3 mL cuvette ($[S]_0 = 200\ \mu M$; $[DTNB]_0 = 500\ \mu M$), and the cuvette is placed in the jacketed cell holder of a Perkin-Elmer Lambda 20 spectrophotometer. Reaction temperature is maintained at 25.0 ± 0.1 °C by a circulating water bath. After the reaction solution reaches thermal equilibrium (∼5 min), data are collected for 5−10 min to allow an accurate estimate to be made of the nonenzymatic rate of thioester hydrolysis. To initiate the enzymatic reaction, 22 μL of stock PBP 2x* is added to the cuvette ($[E]_0 = 0.1\ \mu M$). Sufficient data are collected to estimate the total reaction velocity. Finally, the enzymatic rate is calculated by subtracting the nonenzymatic from the total rate. Data are acquired by a PC that is interfaced to the spectrophotometer.

(B) Measurement of First-Order Progress Curves for PBP 2x-Catalyzed Thioester Hydrolysis. When $[S]_0 \ll K_m$, reaction progress curves are pseudo-first-order in substrate concentration. Product formation for such reactions can be described by the simple expression $[P]_t = [P]_0\{1 - \exp(-k_{obs}t)\}$, where k_{obs} equals $(k_c/K_m)[E]_0$. To apply this method to the PBP 2x-catalyzed hydrolysis of Bz-(D)Ala-^{S}Gly, initial concentrations of substrate and enzyme were generally set at 50 μM and 1 μM, respectively, and product formation was followed for at least three half-lives. Values of k_{obs} were then determined from nonlinear least-squares analysis of the reaction progress curves to the above rate law.

Kinetics of Interaction of PBP 2x with Penicillin G.* Rate constants for the interaction of PBP 2x* with penicillin G were determined by monitoring the decrease in intrinsic tryptophan fluorescence that accompanies acylation of PBP 2x* by penicillin (*7*). For concentrations of penicillin G less than 20 μM, reactions were slow enough that we were able to use a conventional fluorometer. In a typical experiment, 44 μL of stock PBP 2x* was added to 2.00 mL of assay buffer (50 mM MES and 500 mM KCl, pH 6.5) in a 3 mL fluorescence cuvette ($[PBP\ 2x^*]_0 = 0.2\ \mu M$) and the cuvette was placed in the jacketed cell holder of a Hitachi fluorometer. Reaction temperature is maintained at 25.0 ± 0.1 °C by a circulating water bath. After the reaction solution reached thermal equilibrium (∼5 min), baseline fluorescence ($\lambda_{ex} = 290$ nm; $\lambda_{em} = 340$ nm) was recorded for about 5 min. To initiate the reaction, 4 μL of a 1.0 mM freshly prepared stock solution of penicillin G in buffer was added to the cuvette ($[penicillin\ G]_0 = 2\ \mu M$). Under these conditions (i.e., $[penicillin\ G]_0 \gg [PBP\ 2x^*]_0$), the decrease in fluorescence is pseudo-first-order and the rate constant for this process can be calculated by fitting the progress curve to a first-order rate law.

Rapid, Stopped-Flow Kinetic Experiments. Two mechanistic questions required the use of rapid kinetic techniques: Does an acyl-enzyme accumulate during hydrolysis of Bz-(D)Ala-^{S}Gly by PBP 2x*? And, do penicillin G and PBP 2x* form an initial "Michaelis complex" prior to inactivation chemistry? In both cases, acylation of PBP 2x* results in a decrease in the intensity of the intrinsic fluorescence of the protein. The time dependence of these changes was monitored by use of an Applied Photophysics stopped-flow system equipped with fluorescence and temperature-control accessories. Excitation wavelength was set to 290 nm with a monochromator, while the emission was set with a 340 nm cutoff filter. The dead time of this instrument is <2 ms.

RESULTS

Nonenzymatic Hydrolysis of Bz-(D)Ala-^{S}Gly. The thioester substrate Bz-(D)Ala-^{S}Gly undergoes slow but significant hydrolysis in aqueous buffer to produce Bz-(D)Ala and mercaptoacetic acid. The pH dependence of this reaction is shown in Figure 1, where we plot k_{hyd}, the observed pseudo-first-order rate constant for hydrolysis, as a function of pH. As shown in Figure 1, the dependence of k_{hyd} on pH is biphasic and indicates a complex reaction mechanism involving at least two pathways for Bz-(D)Ala-^{S}Gly hydrolysis. At high pH, Bz-(D)Ala-^{S}Gly undergoes hydroxide-dependent hydrolysis, but at pH values below 9, a competing hydroxide-independent reaction becomes the predominant hydrolytic pathway. The data of this figure can be fit to the rate law

$$k_{obs} = k_w + k_{HO}[HO^-] \quad (4)$$

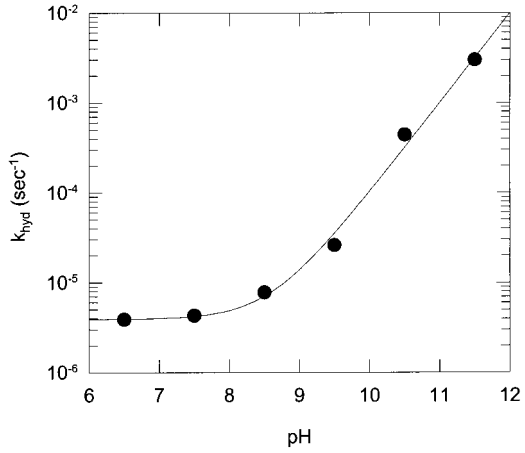

FIGURE 1: pH dependence of the rate constant for aqueous hydrolysis of Bz-(D)Ala-^{S}Gly. At the indicated pH values, initial velocities for thioester hydrolysis were measured by monitoring the decrease in absorbance at 250 nm ($\Delta\epsilon = -2200$). Values of k_{hyd}, calculated by dividing these rates by the substrate concentration, were plotted versus pH as shown here. The solid line through the data points was drawn according to eq 4 and the best-fit parameters: $k_{HO} = 1.04 \pm 0.09$ M^{-1} s^{-1} and $k_w = (2.93 \pm 0.18) \times 10^{-6}$ s^{-1}. Reaction conditions: 50 mM Goods buffer salt and 500 mM KCl; [Bz-(D)Ala-^{S}Gly] = 1.0 mM; 25 °C.

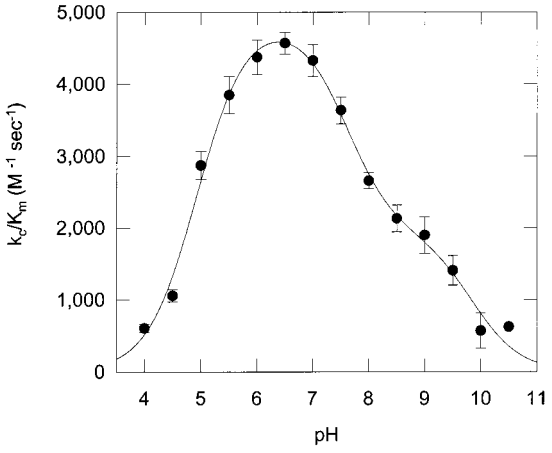

FIGURE 2: pH dependence of k_c/K_m for the PBP 2x*-catalyzed hydrolysis of Bz-(D)Ala-^{S}Gly. Velocities for enzymatic reactions were calculated as described under Materials and Methods and divided by the enzyme and substrate concentrations to provide values of k_c/K_m. These latter values are plotted here as a function of pH. The error bars are standard deviations of means from 3−6 replicate measurements. The solid line was drawn according to eq 5 and the best-fit parameters: $(k_c/K_m)_2 = 4900 + 160$ M^{-1} s^{-1}, $(k_c/K_m)_1 = 1900 \pm 230$ M^{-1} s^{-1}, p$K_{a,3} = 4.93 \pm 0.06$, p$K_{a,2} = 7.61 \pm 0.14$, and p$K_{a,1} = 9.85 \pm 0.18$. Reaction conditions: 50 mM Goods buffer salt and 500 mM KCl; [Bz-(D)Ala-^{S}Gly] = 25 μM; [PBP 2x*] = 0.1 μM; 25 °C.

where k_w is the first-order rate constant for the water or hydroxide-independent reaction and k_{HO} is the second-order rate constant for the hydroxide reaction. Best-fit values for these parameters are $k_w = (2.9 \pm 0.2) \times 10^{-6}$ s^{-1} and $k_{HO} = 1.3 \pm 0.1$ M^{-1} s^{-1}. A similar pH−rate profile has been reported for the hydrolysis of mercaptoacetic acid *p*-nitrobenzoate (*9*), where $k_w = 56 \times 10^{-6}$ s^{-1} and $k_{HO} = 4.7$ M^{-1} s^{-1} (50 °C). The authors of this paper suggest that k_w reflects an intramolecular process in which the free carboxylate acts as a general-base catalyst to promote the attack of water. This is supported in the present case by a solvent deuterium isotope effect on k_w of 1.7 ± 0.1 (data not shown). Simple attack by hydroxide is anticipated to produce an isotope effect of around 0.5, while intramolecular attack by carboxylate anion with formation of an anhydride intermediate would be isotopically silent.

Cloning, Expression, and Purification of PBP 2x.* To conveniently study the mechanism of catalysis by a penicillin binding protein, we cloned, expressed, and purified a His$_6$-tagged version of PBP 2x from *S. pneumoniae* that lacks the N-terminal transmembrane domain (Δ1−50). This protein, PBP 2x*, has been shown to be soluble in simple buffer solutions and catalytically active (*8*). We were able to express PBP 2x* to a level of 30 mg/L and purify it to near homogeneity as judged by SDS−PAGE analysis (data not shown). The PBP 2x* concentrations of stock solutions that were used in this study varied from 9 to 20 μM in 50/50 PBS/glycerol. When stored at −20 °C, these enzyme preparations were found to be stable for at least 9 months.

pH Dependence of k_c/K_m for the PBP 2x-Catalyzed Hydrolysis of Bz-(D)Ala-^{S}Gly.* At pH values that ranged from 4.0 to 10.5, we determined steady-state velocities for the PBP 2x*-catalyzed hydrolysis of Bz-(D)Ala-^{S}Gly at a single substrate concentration of 25 μM. This concentration of substrate is at least 10-fold less than K_m over this pH range (see below), and thus, the measured steady-state velocities equal $(k_c/K_m)[E]_0[S]_0$. Values of k_c/K_m determined in this way are plotted as a function of pH in Figure 2 and depict a bell-shaped dependence with a shoulder on the alkaline side of the bell. The presence of a shoulder indicates that the reaction mechanism involves at least two routes to products. The simplest kinetic mechanism that can account for our results is shown in Scheme 3, in which EH_2 and EH are catalytically active forms of PBP 2x* and EH_3 and E are the catalytically inactive forms that predominate at extremes of acid and alkaline, respectively. The steady-state rate expression that describes the mechanism of Scheme 3 was derived from rapid equilibrium assumptions:

Scheme 3: Mechanism for the pH Dependence of Catalysis of PBP 2x*

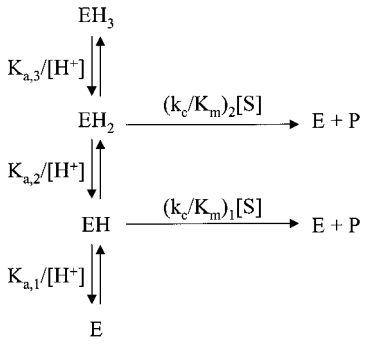

$$k_c/K_m = \frac{(k_c/K_m)_2}{\frac{[H^+]}{K_{a,3}} + 1 + \frac{K_{a,2}}{[H^+]} + \frac{K_{a,2}K_{a,1}}{[H^+]^2}} + \frac{(k_c/K_m)_1}{\frac{[H^+]^2}{K_{a,3}K_{a,2}} + \frac{[H^+]}{K_{a,2}} + 1 + \frac{K_{a,1}}{[H^+]}} \quad (5)$$

The best-fit parameters are summarized in Table 1 and were used to draw the solid line through the data points of Figure 2.

Table 1: Summary of pH Dependencies for PBP 2x* Catalysis and Inactivation[a]

substrate	$k_{E,2}$[b] (mM^{-1} s^{-1})	$k_{E,1}$[b] (mM^{-1} s^{-1})	p$K_{a,3}$	p$K_{a,2}$	p$K_{a,1}$
Bz-(D)Ala-^{S}Gly	4.9 ± 0.2	1.9 ± 0.2	4.9 ± 0.1	7.6 ± 0.1	9.9 ± 0.2
penicillin G	67 ± 4	34 ± 2	5.2 ± 0.1	7.2 ± 0.2	9.9 ± 0.1

[a] Reaction conditions: 50 mM Goods buffer and 500 mM KCl, 25° C. [b] k_E corresponds to k_c/K_m for hydrolysis of Bz-(D)Ala-^{S}Gly and k_{inact}/K_i for inactivation by penicillin G.

pH Dependence of Steady-State Kinetic Parameters for the PBP 2x-Catalyzed Hydrolysis of Bz-(D)Ala-^{S}Gly.* To probe the pH dependence of PBP 2x* catalysis in more detail, we determined the individual steady-state kinetic parameters as a function of pH. At pH values of 4.0, 5.5, 6.5, 7.5, 8.5, and 9.5, we determined the substrate concentration dependence of steady-state velocities for the PBP 2x*-catalyzed hydrolysis of Bz-(D)Ala-^{S}Gly ($0.25\ mM \leq [S]_0 \leq 2.5\ mM$). In all cases, the dependence of v_{ss} on $[S]_0$ obeyed the simple Michaelis−Menten equation and provided the best-fit values of k_c, k_c/K_m, and K_m that are plotted as a function of pH in Figure 3, panels A−C, respectively.

The pH dependence of k_c, like that of k_c/K_m, is bell-shaped with a shoulder.[2] While the shoulder is on the acidic side of the bell for k_c, the pH dependence of k_c still adheres to a mechanism that is analogous to the mechanism for k_c/K_m shown in Scheme 3. Given this, we expanded the mechanism of Scheme 3 to include isomerizations of the enzyme−substrate complex as well as the substrate binding and turnover steps as shown in Scheme 4. Estimates for the parameters of Scheme 4 are summarized in Table 2 and were arrived at in the following way. The three acid dissociation constants for the four forms of free enzyme (i.e., p$K_{a,3}$, p$K_{a,2}$, and p$K_{a,1}$), $(k_c/K_m)_2$, and $(k_c/K_m)_1$ are best-fit values from the dependence of k_c/K_m on pH according to eq 5. The three acid dissociation constants for the four forms of substrate-complexed enzyme (i.e., p$K_{a,3}'$, p$K_{a,2}'$, and p$K_{a,1}'$), $k_{c,2}$ and $k_{c,1}$ are best-fit values from the dependence of k_c on pH according to an analogous form of eq 5. Finally, $K_{m,2}$ and $K_{m,1}$ are simply the ratio of the corresponding values of k_c and k_c/K_m.

Solvent Deuterium Isotope Effects for the PBP 2x-Catalyzed Hydrolysis of Bz-(D)Ala-^{S}Gly.* To probe features of the rate-limiting transition state for PBP 2x* catalysis, we determined solvent deuterium isotope effects on the steady-state kinetic parameters. Figure 4A shows our experiments at pH 6.5 and pD equivalent. The substrate concentration dependencies of steady-state velocities were determined for the PBP 2x*-catalyzed hydrolysis of Bz-(D)Ala-^{S}Gly in light and heavy water, and the resultant data sets were fit to a simple rearrangement of the Michaelis−Menten equation that allows direct access to k_c and k_c/K_m:

$$v_{ss} = \frac{[S]_0[E]_0}{(k_c/K_m)^{-1} + [S]_0 k_c^{-1}} \qquad (6)$$

The best-fit parameters are, for H_2O, $k_c = 4.39 \pm 0.28\ s^{-1}$ and $k_c/K_m = 4740 \pm 480\ M^{-1}\ s^{-1}$; and for D_2O, $k_c = 2.00 \pm 0.09\ s^{-1}$ and $k_c/K_m = 2760 \pm 220\ M^{-1}\ s^{-1}$. Solvent isotope effects on k_c and k_c/K_m were calculated from these results at pH 6.5 and are summarized in Table 3 along with the solvent isotope effects that were determined at pH 9.0. Note that the isotope effects at pH 6.5 reflect reaction of the enzyme species EH_2 (see Scheme 3) while the isotope effect at pH 9.0 reflects reaction of EH. Taken together, these results suggest that, for the PBP 2x*-catalyzed hydrolysis of Bz-(D)Ala-^{S}Gly, both k_c and k_c/K_m for the two reaction paths to product are rate-limited by reaction steps involving protolytic catalysis.

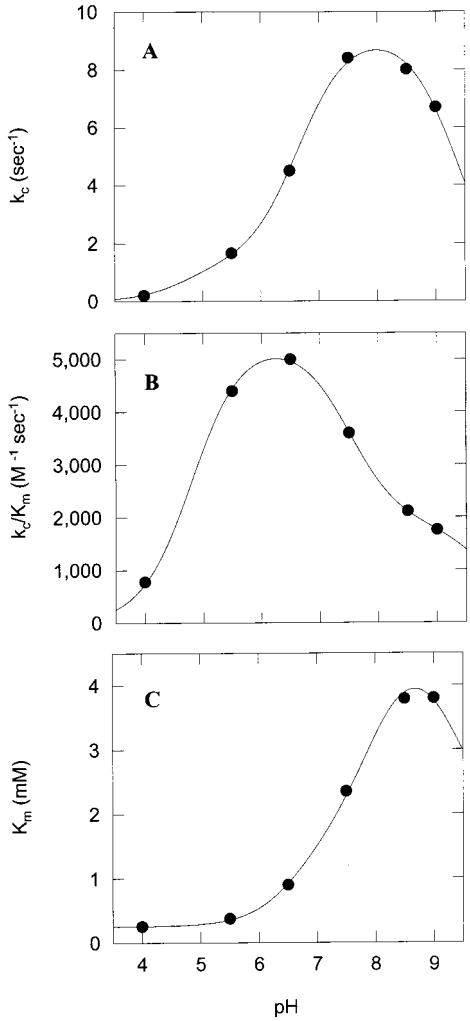

FIGURE 3: pH dependence of steady-state kinetic parameters for the PBP 2x*-catalyzed hydrolysis of Bz-(D)Ala-^{S}Gly. At the indicated pH values, the dependence of steady-state velocity on substrate concentration was determined for the PBP 2x*-catalyzed hydrolysis of Bz-(D)Ala-^{S}Gly. From these dependencies, values of k_c, K_m, and k_c/K_m were determined by nonlinear least-squares fit to the Michaelis−Menten equation and the resultant values were plotted versus pH. (A) k_c vs pH. Line was drawn according to eq 5 and best-fit values: $k_{c,2} = 1.35 \pm 0.86\ s^{-1}$, $k_{c,1} = 9.36 \pm 0.38\ s^{-1}$, p$K_{a,3} = 4.70 \pm 0.90$, p$K_{a,2} = 6.66 \pm 0.14$, and p$K_{a,1} = 9.36 \pm 0.10$. (B) k_c/K_m vs pH. Line was drawn according to eq 5 and best-fit values: $(k_c/K_m)_2 = 5360 \pm 108\ M^{-1}\ s^{-1}$, $(k_c/K_m)_1 = 1900 \pm 220\ M^{-1}\ s^{-1}$, p$K_{a,3} = 4.80 \pm 0.05$, p$K_{a,2} = 7.51 \pm 0.08$, and p$K_{a,1} = 9.92 \pm 0.51$. (C) K_m vs pH. Line was drawn according to the ratio of expressions for the pH dependencies of k_c and k_c/K_m and the above values. Reaction conditions: 50 mM Goods buffer salt and 500 mM KCl; $0.25\ mM \leq$ [Bz-(D)Ala-^{S}Gly] ≤ 5.0 mM; [PBP 2x*] = 0.1 μM; 25 °C.

Proton Inventory for k_c/K_m for the PBP 2x-Catalyzed Hydrolysis of Bz-(D)Ala-^{S}Gly.* To probe the acylation of PBP

[2] It should be noted that attempts at fitting the data sets of Figure 3 to models having only two ionizable groups resulted in fits of extremely poor quality relative to the fits that are shown.

Scheme 4: Mechanism for the pH Dependence of Catalysis by PBP 2x*

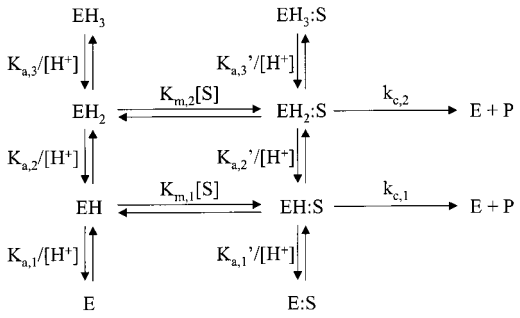

Table 2: Estimates of Steady-State Kinetic Parameters for the PBP 2x*-Catalyzed Hydrolysis of Bz-(D)Ala-^{S}Gly

parameter	value	parameter	value
p$K_{a,3}$	4.8 ± 0.1	p$K_{a,3}'$	4.7 ± 0.9
p$K_{a,2}$	7.5 ± 0.1	p$K_{a,2}'$	6.7 ± 0.1
p$K_{a,1}$	9.9 ± 0.5	p$K_{a,1}'$	9.4 ± 0.1
$K_{m,2}$ (mM)	0.25	$k_{c,2}$ (s^{-1})	1.4 ± 0.9
$K_{m,1}$ (mM)	5	$k_{c,1}$ (s^{-1})	9.4 ± 0.4
		$(k_c/K_m)_2$ (mM^{-1} s^{-1})	5.4 ± 0.1
		$(k_c/K_m)_1$ (mM^{-1} s^{-1})	1.9 ± 0.2

2x* by Bz-(D)Ala-^{S}Gly, we determined the proton inventory for k_c/K_m. In proton inventory experiments, a kinetic parameter is determined as a function of mole fraction of solvent deuterium, n_{D_2O} (*10*). The shape of the dependence of rate constant on n_{D_2O} is diagnostic of certain mechanistic features. The data for the hydrolysis of Bz-(D)Ala-^{S}Gly by PBP 2x* are shown in Figure 4B, where we see a "dome-shaped" proton inventory. Analysis of these results is presented in the Discussion section.

*Accumulation of Acyl-Enzyme during the Hydrolysis of Bz-(D)Ala-^{S}Gly by PBP 2x**. An important mechanistic question is whether an acyl-enzyme accumulates in the steady state during the PBP 2x*-catalyzed hydrolysis of Bz-(D)Ala-^{S}Gly. To answer this question, we conducted rapid kinetic experiments in which we mixed enzyme with substrate in a stopped-flow apparatus and monitored the intrinsic fluorescence of the protein. The fluorescence tracing of a typical experiment is shown in Figure 5 and illustrates that rapid mixing of enzyme and substrate is followed by a first-order decrease in fluorescence intensity. Fluorescence changes of this sort have been observed for the acylation of PBP 2x* by penicillin G and another thioester substrate, Bz-Gly-^{S}Ala (*7*), and thus suggested to us that the observed fluorescence change that we see here is due to acylation by Bz-(D)Ala-^{S}Gly.

The observed first-order rate constant calculated from such data has the dependence on substrate concentration that is shown in Figure 6. These data can be fit to the rate expression of eq 4, where the kinetic constants take their meaning from Scheme 2:

$$k_{obs} = \frac{k_{acyl}[S]}{K_s + [S]} + k_{deacyl} \qquad (7)$$

Nonlinear fitting of the data of Figure 6 to eq 7 provides the following best-fit values: $K_s = 4.1 \pm 1.4$ mM, $k_{acyl} = 19 \pm 3$ s^{-1}, and $k_{deacyl} = 8.4 \pm 1.2$ s^{-1}. These values, together with eqs 2 and 3, allow calculation of steady-state parameters

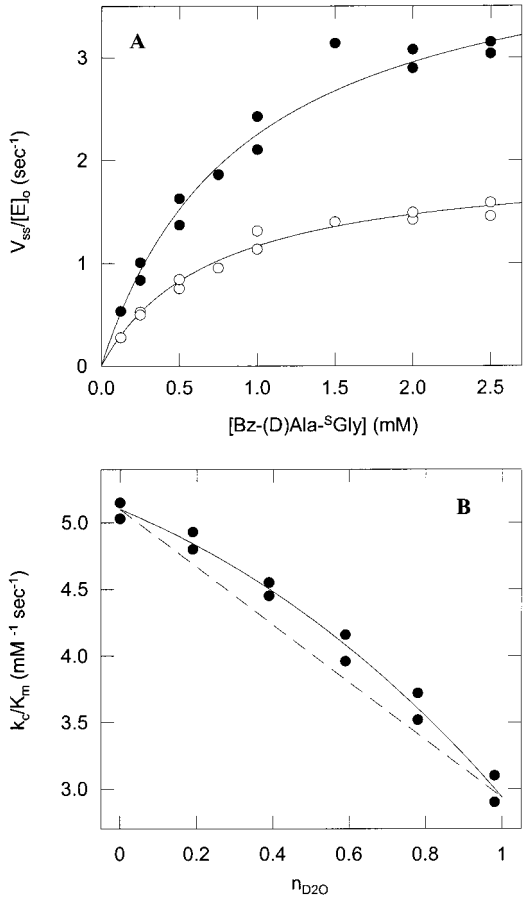

FIGURE 4: Solvent deuterium isotope effects for the PBP 2x*-catalyzed hydrolysis of Bz-(D)Ala-^{S}Gly. (A) Substrate concentration dependence of steady-state velocities was determined for the PBP 2x*-catalyzed hydrolysis of Bz-(D)Ala-^{S}Gly in light and heavy water (● and ○, respectively). The data are plotted here along with lines drawn according to eq 6 and the following best-fit parameters: for H_2O, kc = 4.39 ± 0.28 s^{-1} and k_c/K_m = 4740 ± 480 M^{-1} s^{-1}; for D_2O, k_c = 2.00 ± 0.09 s^{-1} and k_c/K_m = 2760 ± 220 M^{-1} s^{-1}. Reaction conditions: 0.25 mM ≤ [Bz-(D)Ala-^{S}Gly] ≤ 5.0 mM; [PBP 2x*] = 0.1 μM; 25 °C. (B) As a function of mole fraction solvent deuterium, values of k_c/K_m were determined from full first-order progress curves collected at $[S]_0 = 50$ μM and $[E]_0 = 1$ μM. The solid line through the data was drawn according to eq 16 and the best-fit parameters: $Z = 1.43 \pm 0.11$, $\phi^T = 0.401 \pm 0.036$, and $k_0 = 5.10 \pm 0.6$ mM^{-1} s^{-1}. The dashed line illustrates the departure of the data from linearity. Reaction conditions: 50 mM MES and 500 mM KCl, pH 6.5 and pD equivalent, T = 25 °C.

Table 3: Solvent Deuterium Isotope Effects for PBP 2x* Catalysis and Inactivation[a]

substrate	pH	$^{D_2O}k_c$	$^{D_2O}(k_c/K_m)$
Bz-(D)Ala-^{S}Gly	9.0	2.43 ± 0.21	1.70 ± 0.07
Bz-(D)Ala-^{S}Gly	6.5	2.20 ± 0.02	1.72 ± 0.05
penicillin G[b]	6.5		1.25 ± 0.08

[a] Reaction conditions: For the hydrolysis of Bz-(D)Ala-^{S}Gly at pH 6.5, 0.25 mM ≤ [Bz-(D)Ala-^{S}Gly] ≤ 5.0 mM, [PBP 2x*] = 0.1 μM; 50 mM MES and 500 mM KCl, pH 6.5 and pD equivalent, 25 °C. For the hydrolysis of Bz-(D)Ala-^{S}Gly at pH 9.0, 0.25 mM ≤ [Bz-(D)Ala-^{S}Gly] ≤ 5.0 mM, [PBP 2x*] = 0.1 μM; 50 mM CHES and 500 mM KCl, pH 9.0 and pD equivalent, 25 °C. For inactivation by penicillin G, [penicillin G] = 2 μM, [PBP 2x*] = 0.2 μM, 50 mM MES, 500 mM KCl, pH 6.5 and pD equivalent, 25 °C. [b] For penicillin G, the solvent isotope effect was measured for k_{inact}/K_i.

$k_c = 5.8$ s^{-1} and $K_m = 1.4$ mM. Significantly, these values are nearly identical to values that were determined indepen-

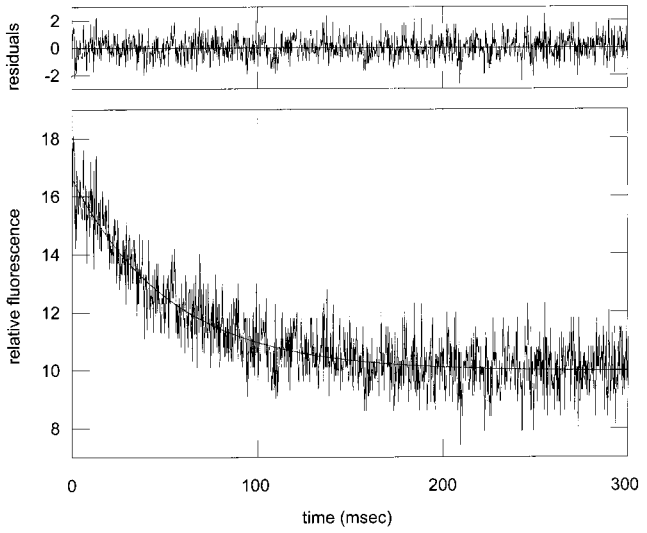

FIGURE 5: Progress curve for the pre-steady-state accumulation of an acyl-enzyme during the hydrolysis of Bz-(D)Ala-^{S}Gly by PBP 2x*. In this rapid kinetics experiment, a 5 mM solution of Bz-(D)-Ala-^{S}Gly in assay buffer was mixed with a 0.5 μM solution of PBP 2x* in a stopped-flow apparatus and the intrinsic fluorescence of the enzyme (λ_{ex} = 290 nm; λ_{em} = 340 nm) was monitored as a function of time. The decrease in fluorescence intensity that is observed upon mixing substrate and enzyme can be described by a simple exponential dependence on time with a first-order rate constant of 18.9 ± 0.5 s^{-1}. Reaction conditions: 50 mM MES and 500 mM KCl, pH 6.5; [Bz-(D)Ala-^{S}Gly] = 2.5 mM; [PBP 2x*] = 0.25 μM; 25 °C.

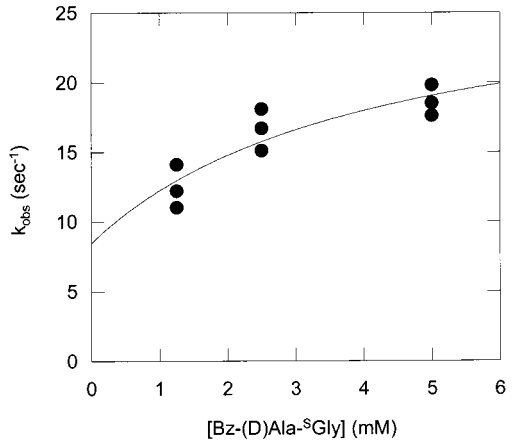

FIGURE 6: Substrate concentration dependence of the observed, pseudo-first-order rate constant for the pre-steady-state reaction of Bz-(D)Ala-^{S}Gly and PBP 2x*. Values of k_{obs} were determined as outlined in the Materials and Methods section and plotted here as a function of substrate concentration. The solid line was drawn according to eq 7 and the best-fit parameters: K_s = 4.1 ± 1.4 mM, k_{acyl} = 19 ± 3 s^{-1}, and k_{deacyl} = 8.4 ± 1.2 s^{-1}. Reaction conditions: 50 mM MES and 500 mM KCl, pH 6.5; [PBP 2x*] = 0.25 μM; 25 °C.

dently in several steady-state kinetic experiments, k_c = 4.9 ± 0.1 s^{-1} and K_m = 1.1 ± 0.2 mM (n = 5).

Inactivation of PBP 2x by Penicillin G.* Figure 7 shows titration data for the inactivation of PBP 2x* by penicillin G. In this experiment, aliquots of PBP 2x* at a nominal concentration of 200 nM were allowed to react with various concentrations of penicillin G for 30 min. At the end of this time, residual activity was measured by use of Bz-(D)Ala-^{S}Gly and plotted as a function of the concentration of penicillin G. These data describe a straight line with an x-axis

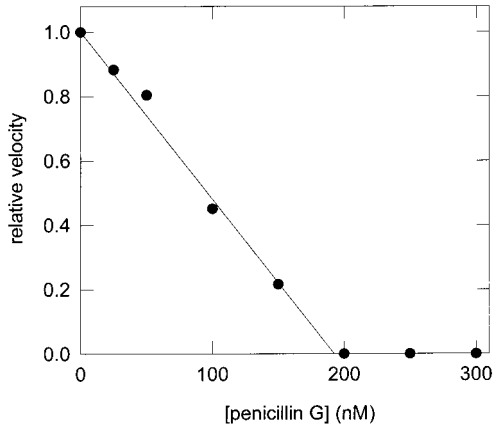

FIGURE 7: Titration of PBP 2x* by penicillin G. The indicated concentration of penicillin G were incubated for 30 min with a nominal concentration of 200 nM PBP 2x* in assay buffer (50 mM MES and 500 mM KCl, pH 6.5) at 25 °C, and the residual enzyme activity was measured with 1 mM Bz-(D)Ala-^{S}Gly.

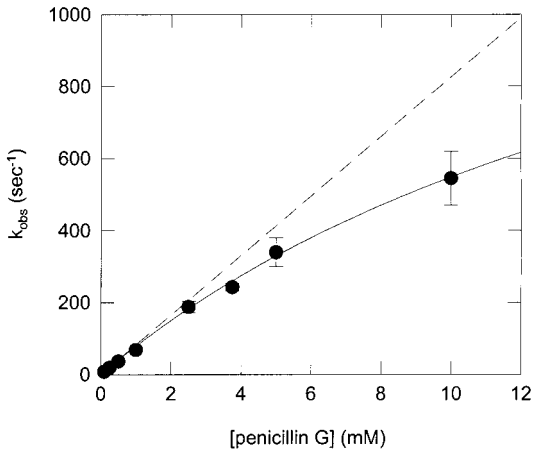

FIGURE 8: Inhibitor concentration dependence for the inactivation of PBP 2x* by penicillin G. Values of k_{obs} for the interaction of PBP 2x* with penicillin G were determined as outlined in the Materials and Methods section. The solid line was drawn through the data according to the expression of eq 8 and the best-fit parameters: k_{inact} = 1600 ± 300 s^{-1} and K_i = 20 ± 5 mM. The dashed line was drawn according to the ratio k_{inact}/K_i of 83 mM^{-1} s^{-1} and was included in this figure to illustrate the departure of the data from a simple linear dependence. Reaction conditions: 50 mM MES and 500 mM KCl, pH 6.5; [PBP 2x*] = 0.5 μM; 25 °C.

intersect of 195 nM and indicate irreversible and stoichiometric inhibition of PBP 2x* by penicillin G.

Saturation Kinetics for the Inactivation of PBP 2x by Penicillin G.* As a first step toward defining the mechanism of inactivation of PBP 2x* by penicillin G, we wanted to determine if a Michaelis complex forms prior to acylation of PBP 2x* by penicillin G and, if so, to estimate the dissociation constant for this complex. To this end, we determined the dependence of k_{obs}, the pseudo-first-order inactivation rate constant, on penicillin G concentration. Values of k_{obs} were determined by monitoring the change in intrinsic protein fluorescence that accompanies acylation by penicillin. The dependence of k_{obs} on penicillin G concentration is shown in Figure 8 and can be described by

$$k_{obs} = \frac{k_{inact}[I]}{[I] + K_i} \quad (8)$$

where K_i is the dissociation constant for accumulation of

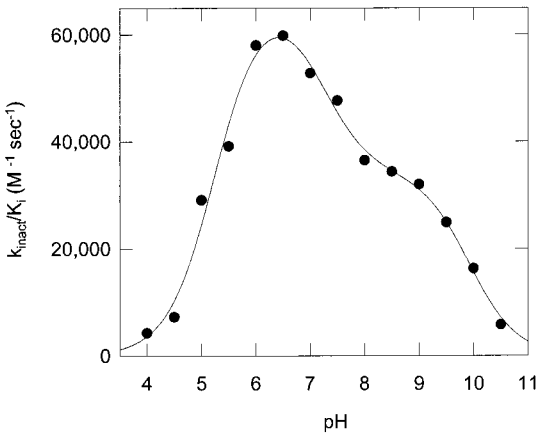

FIGURE 9: pH dependence of k_{inact}/K_i for the inactivation of PBP 2x* by penicillin G. Values of k_{obs} for the interaction of PBP 2x* with penicillin G were determined as outlined in the Materials and Methods section and were divided by penicillin G concentration to provide k_{obs}/[I], which, under these conditions, equals k_{inact}/K_i. These latter values are plotted here as a function of pH. As a practical matter, the concentration of penicillin G was chosen to provide conveniently measured values of k_{obs} of around 0.05 s^{-1}. The dependence of k_{inact}/K_i on pH is shown here together with the best-fit line according to eq 5 and the parameter estimates: $(k_{inact}/K_i)_2 = 67 \pm 4$ mM^{-1} s^{-1}, $(k_{inact}/K_i)_1 = 34 \pm 2$ mM^{-1} s^{-1}, $pK_{a,3} = 5.24 \pm 0.08$, $pK_{a,2} = 7.23 \pm 0.21$, and $pK_{a,1} = 9.93 \pm 0.13$. Reaction conditions: 50 mM Goods buffer salt and 500 mM KCl; 2 μM $\leq$ [penicillin G] $\leq$ 12 μM; [PBP 2x*] = 0.2 μM; 25 °C.

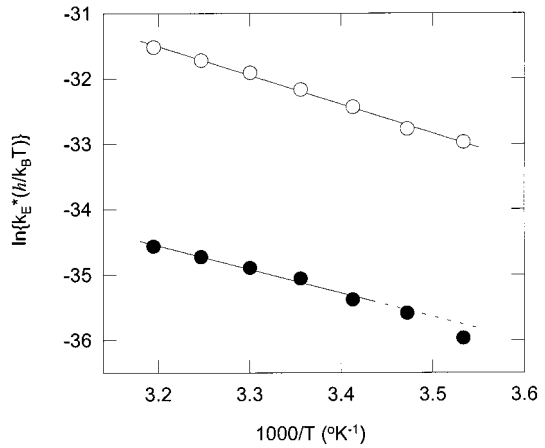

FIGURE 10: Temperature dependence of acylation of PBP 2x* by penicillin G and Bz-(D)Ala-^{S}Gly. Values of k_c/K_m for the PBP 2x-catalyzed hydrolysis of Bz-(D)Ala-^{S}Gly and k_{inact}/K_i for the inactivation of PBP 2x by penicillin G were determined as described in the text. These second-order rate constants were normalized to a standard state of 1 μM to produce values of k_E*, which are plotted here as their dependence on reciprocal absolute temperature (○, inactivation by penicillin G; ●, hydrolysis of Bz-(D)Ala-^{S}Gly). The solid lines were drawn according to the best-fit values to eq 11: for penicillin G, slope = -4421 ± 131 T^{-1} and *y*-intercept = -17.36 ± 0.44; for Bz-(D)Ala-^{S}Gly, slope = -3603 ± 144 T^{-1} and *y*-intercept = -23.03 ± 0.92. Reaction conditions: 50 mM MES and 500 mM KCl, pH = 6.5.

the Michaelis complex of enzyme and inhibitor and k_{inact} is the first-order rate constant that governs the chemical transformation of this complex into the final, irreversibly formed enzyme−inhibitor species. When the data of Figure 8 were fit to eq 8, the following best-fit parameters were found: $k_{inact} = 1600 \pm 300$ s^{-1}, $K_i = 20 \pm 5$ mM, and $k_{inact}/K_i = 83 \pm 7$ mM^{-1} s^{-1}.

pH dependence for the Inactivation of PBP 2x by Penicillin G.* The pH dependence of k_{inact}/K_i for the inactivation of PBP 2x* by penicillin G is shown in Figure 9. To conveniently determine values of k_{inact}/K_i, we measured k_{obs} at low concentrations of penicillin G (2−12 μM) that are much less than the estimate of K_i of greater than 20 mM (see above). Under these conditions, k_{inact}/K_i can be calculated as the simple ratio k_{obs}/[I].

The pH dependence of k_{inact}/K_i is identical in shape to the pH dependence of k_c/K_m (see Figure 2) and thus suggests similar mechanisms for the two reactions. This allowed us to fit the data to a rate expression analogous to that of eq 5. The best-fit values are summarized in Table 1.

Solvent Deuterium Isotope Effects for the Inactivation of PBP 2x by Penicillin G.* To explore mechanistic details of the inactivation of PBP 2x* by penicillin G, we determined solvent deuterium isotope effects on k_{inact}/K_i. Triplicate values of k_{obs} were determined at [penicillin G] = 2 μM and [PBP 2x*] = 0.2 μM in light and heavy water [pH = 6.5 and pD equivalent (*10*)]. From these values we calculated the following: for H_2O, $k_{inact}/K_i = 58.1 \pm 1.3$ mM^{-1} s^{-1}; for D_2O, $k_{inact}/K_i = 46.5 \pm 2.6$ mM^{-1} s^{-1}; $^D(k_{inact}/K_i) = 1.25 \pm 0.08$.

Temperature Dependence of Acylation of PBP 2x by Bz-(D)Ala-^{S}Gly and Penicillin G.* To further explore mechanistic similarities and differences in the reaction of PBP 2x with Bz-(D)Ala-^{S}Gly and penicillin G, we determined activation parameters for these reactions from their temperature dependencies. For hydrolysis of Bz-(D)Ala-^{S}Gly by PBP 2x, values of k_c/K_m were determined as described under Materials and Methods and multiplied by a standard-state enzyme concentration of 1 μM to arrive at values of the normalized, first-order rate constant, k_E*. Likewise, for inactivation of PBP 2x by penicillin G, values of k_{inact}/K_i were determined and multiplied by a standard-state inactivator concentration of 1 μM to arrive at similarly normalized first-order rate constants. In both cases

$$k_E^* = \frac{k_b T}{h} \exp\left(-\frac{\Delta G^{\ddagger}}{RT}\right) \tag{9}$$

where $\Delta G^{\ddagger}$ is the Gibbs free energy of activation and k_b, h, and R are the Boltzmann, Planck, and gas constants, respectively. The expression of eq 9 can be recast in familiar thermodynamic form as

$$k_E^* = \frac{k_b T}{h} \exp\left[-\left(\frac{\Delta H^{\ddagger}}{RT} - \frac{\Delta S^{\ddagger}}{R}\right)\right] \tag{10}$$

where $\Delta H^{\ddagger}$ and $\Delta S^{\ddagger}$ are the enthalpy and entropy of activation, respectively. Finally, eq 10 can be rearranged to

$$\ln\left[k_E^*\left(\frac{h}{k_b T}\right)\right] = -\frac{\Delta H^{\ddagger}}{RT} + \frac{\Delta S^{\ddagger}}{R} \tag{11}$$

Equation 11 describes the situation for a kinetically simple process in which one observes a linear dependence of ln k_{obs} on inverse temperature with slope and intercept proportional to $\Delta H^{\ddagger}$ and $\Delta S^{\ddagger}$, respectively.

For acylation of PBP 2x by penicillin G, such a linear dependence is observed (Figure 10), which allows us to calculate $\Delta H^{\ddagger} = 8.8 \pm 0.3$ kcal/mol and $T\Delta S^{\ddagger} = -10.3 + 0.3$ kcal/mol ($T = 298$ K). For acylation of PBP 2x by Bz-(D)Ala-^{S}Gly, we observed linearity in the temperature range

20−40 °C and calculate from these data $\Delta H^{\ddagger} = 7.2 \pm 0.4$ kcal/mol and $T\Delta S^{\ddagger} = -13.7 \pm 0.4$ kcal/mol ($T = 298$ K). The data points at 10 and 15 °C were not included in the calculation but are included in the figure to show the departure from a linear dependence. While this curvature may be mechanistically significant, we lack sufficient data to justify more extensive analysis and detailed interpretation.

DISCUSSION

*Active-Site Chemistry of PBP 2x**. The results of our pre-steady-state kinetic experiments support a mechanism for the PBP 2x*-catalyzed hydrolysis of Bz-(D)Ala-^{S}Gly that involves an acyl-enzyme intermediate (see Scheme 1). Two experimental findings are relevant. First, after rapidly mixing enzyme and Bz-(D)Ala-^{S}Gly, we observe a new enzyme species that has reduced fluorescence intensity relative to unreacted enzyme. Identical fluorescence results are obtained when PBP 2x* is acylated either by β-lactam antibiotics or by the substrate Bz-Gly-^{S}Ala (*7*). Second, this intermediate forms and decomposes with kinetics that are consistent with the acyl-enzyme mechanism of Scheme 1 and the steady-state kinetic parameters that were determined in independent experiments.

In an effort to understand the chemistry of how this acyl-enzyme forms and decomposes, we determined pH dependencies and solvent kinetic isotope effects for PBP 2x* catalysis and inactivation. The pH dependence of k_c/K_m for hydrolysis of Bz-(D)Ala-^{S}Gly suggests a complex mechanism involving two pathways to product and three catalytically essential ionizable groups with pK_a values of 4.9, 7.6, and 9.9 (see Scheme 3).[3] Solvent deuterium isotope effects of 1.7 on both $(k_c/K_m)_2$ and $(k_c/K_m)_1$ suggest similar transition-state structures for the two reaction paths, each path involving an at least partially rate-limiting step that is subject to protolytic catalysis. This step is likely general base-catalyzed attack of the active-site serine on the carbonyl carbon of the substrate. In proposing this transition-state structure for acylation, we assume that expulsion of the thiol leaving group from the tetrahedral intermediate that forms on the reaction pathway to the acyl-enzyme is faster than expulsion of the active-site serine to regenerate free enzyme and substrate (*11*). Thus, we propose as rate-limiting the transition state for general base-catalyzed attack of serine hydroxyl on the carbonyl of the substrate.

An identical dependence of k_{inact}/K_i on pH is observed for the inactivation of PBP 2x* by penicillin G. This suggests that the same ionizable residues that are critical for acylation by substrate are also critical for acylation by β-lactams and that these residues play the same chemical roles in the two reactions. A solvent isotope effect of 1.25 was observed for k_{inact}/K_i and, like the solvent isotope effect on k_c/K_m, suggests that this process is at least partially rate-limited by the chemistry of acylation (see below for a more complete interpretation of these isotope effects).

It is clearly of some interest to establish the identity of the three critical ionizing residues of PBP 2x* and their roles in promoting acylation by Bz-(D)Ala-^{S}Gly and penicillin G. Now, if we consider the likely acylation mechanism of PBP 2x* in the most general sense, one can identify three chemical tasks that need to be accomplished and are appropriate for ionizable amino acid residues: (i) activation of the hydroxyl of the active-site serine for nucleophilic attack, (ii) stabilization of the oxyanion of the tetrahedral transition state and/or intermediate that forms on the pathway to acyl-enzyme, and (iii) binding of the substrate/inhibitor carboxylate moiety to stabilize reaction intermediates. Of course, these three reaction tasks are not exhaustive. In particular, one must always leave open the possibility that a particular ionization is not in the active site but is at some remote site on the protein surface and perhaps plays a role in triggering isomerization of the protein to a conformation that is more or less reactive toward acylation.

The availability of X-ray crystallographic data for the covalent complex of PBP 2x* and the β-lactam antibiotic cefuroxime (*6*) should help us move from these very general considerations to a more refined model and, in fact, does suggest a number of important active-site interactions: (i) The hydroxyl of Ser^{337} functions as nucleophile in reactions of PBP 2x*. The nucleophilicity of this hydroxyl is enhanced by Lys^{340}, which functions as a general base. An extended hydrogen-bonding network may exist around Ser^{337} and Lys^{340} involving Ser^{395}, Asn^{397}, and Lys^{547}. (ii) Hydrogen bonds from the main-chain amides of Ser^{337} and Thr^{550} comprise the "oxyanion hole" of PBP 2x*. (iii) The free carboxylate moiety of the inhibitor is bound through hydrogen-bonding interactions with the hydroxyls of Ser^{548} and Thr^{550}.

This structural information together with the general mechanistic features that we identified above now allows us to formulate the mechanistic proposal for the pH dependence of acylation of PBP 2x* shown in Scheme 5. Note that while Scheme 5 specifically depicts acylation by substrate Bz-(D)Ala-^{S}Gly, it applies with equal validity to acylation by penicillin G. In this mechanism, B, X, and Y correspond to Lys^{340}, Ser^{548} or Thr^{550}, and an enzyme residue whose ionization triggers a conformational transition. To explain this mechanism, we start with the more reactive form of the enzyme, which predominates at pH 6.5 and has a k_c/K_m value of 4900 M^{-1} s^{-1}. As the pH is lowered from 6.5, residue B becomes protonated (pK_a = 4.9), can no longer function as a general base, and generates an inactive form of enzyme. Again starting with the more reactive form of the enzyme at pH 6.5, if the pH is increased, the protonated residue HY ionizes with a pK_a of 7.6 to give rise to a conformational isomer of the enzyme that possesses slightly reduced reactivity. Finally, if the pH is raised still higher, Ser^{548} or Thr^{550} ionizes and thus can no longer hydrogen-bond to the free carboxylate moiety.

This mechanism posits two unusual pK_a values: a pK_a of 5 for the ϵ-amine of Lys^{340} and a pK_a of 10 for the hydroxyl of Ser^{548} or Thr^{550}. While pK_a perturbations of this magnitude are unusual, they do find ample precedent in the literature for active-site residues that are involved in hydrogen-bonding networks (*12*). In addition to these two active-site ionizations, we also suggest that an ionization outside of the active site that influences catalytic efficiency in a subtle way, possibly through a conformational isomerization that alters active-site geometry. While speculative, this suggestion is analogous to allosteric mechanisms. In this case, we simply posit that the allosteric effector is a proton.

[3] We know that all three ionizable groups are on the enzyme since the only ionizable group of the substrate (i.e., the N-terminal carboxylic acid) has a pK_a of around 2.8 (*9*).

Scheme 5: Mechanistic Proposal for the pH Dependence of k_c/K_m for PBP 2x* Catalysis

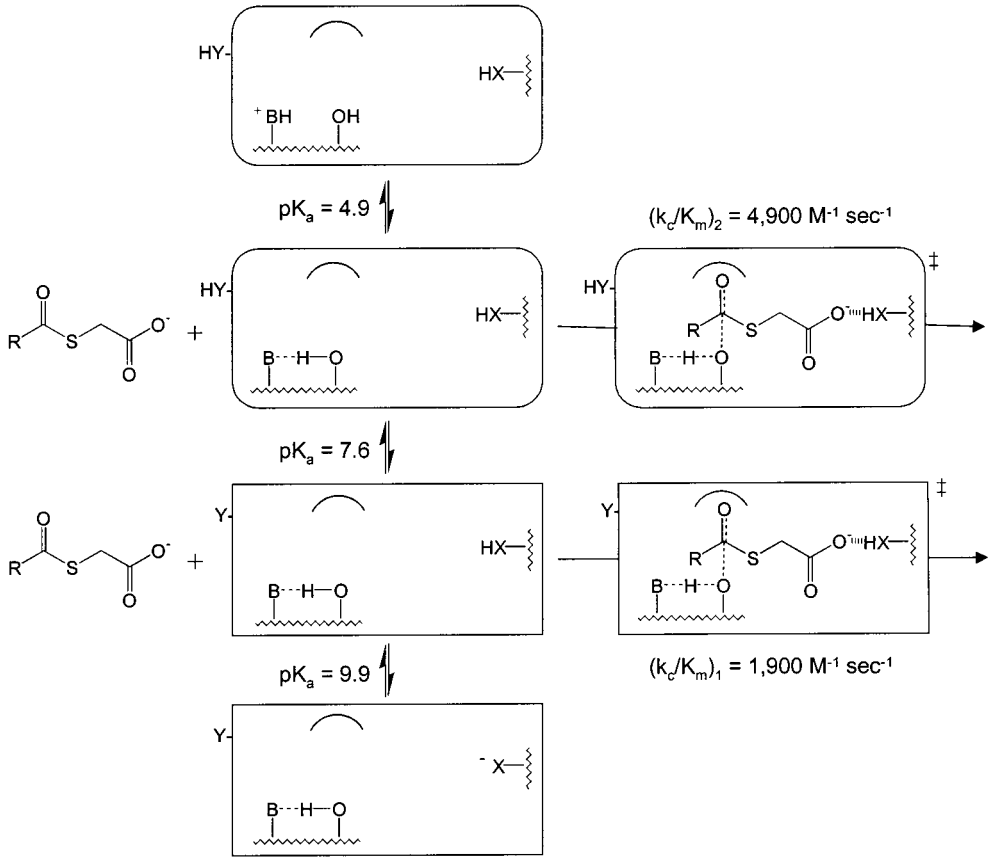

This basic mechanism can be expanded to account for the pH dependence of k_c for the hydrolysis of Bz-(D)Ala-^{S}Gly. Recall that for k_c we see a bell-shaped profile with a shoulder as we saw for k_c/K_m, but now maximal activity occurs at pH 8 and the shoulder is on the acidic side of this maxima. These results can be explained by a pH-dependent change in rate-limiting step in the mechanism of Scheme 6. k_c is equal to $k_{acyl}k_{deacyl}/(k_{acyl} + k_{deacyl})$, where k_{acyl} and k_{deacyl} have the following pH-dependent forms:

$$k_{acyl} = \frac{k_{acyl,2}}{\frac{[H^+]}{K_{a,3}'} + 1 + \frac{K_{a,2}'}{[H^+]} + \frac{K_{a,2}'K_{a,1}'}{[H^+]^2}} + \frac{k_{acyl,1}}{\frac{[H^+]^2}{K_{a,3}'K_{a,2}'} + \frac{[H^+]}{K_{a,2}'} + 1 + \frac{K_{a,1}'}{[H^+]}} \quad (12)$$

$$k_{deacyl} = \frac{k_{deacyl,2}}{\frac{[H^+]}{K_{a,3}''} + 1 + \frac{K_{a,2}''}{[H^+]}} + \frac{k_{deacyl,1}}{\frac{[H^+]^2}{K_{a,3}''K_{a,2}''} + \frac{[H^+]}{K_{a,2}''} + 1} \quad (13)$$

While this expression for k_c is too complex to provide a unique fit to the data of Figure 3A by nonlinear least-squares analysis, we were able to manually adjust the rate and dissociation constants to yield a good fit to these data. These adjustments were performed under the constraint of three conditions: (1) $K_{a,3}'$, $K_{a,2}'$, and $K_{a,1}'$ are set equal to $K_{a,3}$, $K_{a,2}$, and $K_{a,1}$, respectively. With this condition we assume that the binding of substrate to the active site does not alter these dissociation constants. (2) Either EH-acyl does not deprotonate to form E-acyl or, if EH-acyl does deprotonate to E-acyl, both species deacylate with identical rate constants. This reflects a mechanistic feature discussed above that $K_{a,1}$ involves an ionization that is important for binding the carboxylate of the ^{S}Gly moiety of the substrate. Since the acyl-enzyme lacks this moiety, we need not consider this ionization. For simplicity, we omitted the ionization term $K_{a,1}'''$ from the model of Scheme 6 and, thus, from the expression of eq 13 for the pH dependence of deacylation. (3) At pH 6.5, our model must allow us to calculate values for k_{acyl} and k_{deacyl} that are numerically identical to those that we determined experimentally at this pH from our stopped-flow experiments; that is, approximately 19 and 8 s^{-1}, respectively.

Given the above conditions, we were able to manually fit the data of Figure 3A with the following values: $k_{acyl,2}$ = 25 s^{-1}, $k_{deacyl,2}$ = 2 s^{-1}, $k_{acyl,1}$ = 12 s^{-1}, $k_{deacyl,1}$ = 19 s^{-1}, $K_{a,3}'''$ = 4.7, and $K_{a,2}'''$ = 7.0. Figure 11 displays the pH-dependent data and the theoretical line that was drawn with these parameters as well as separate, theoretical lines for the pH dependence of k_{acyl} and k_{deacyl}. The fit of the line through the data is excellent and inspection of the curves for k_{acyl} and k_{deacyl} reveals that, at pH 6.5, k_{acyl} = 22 s^{-1} and k_{deacyl} = 6 s^{-1}, respectively, in good agreement with the experimentally determined values from our pre-steady-state experiments.

Finally, we were able to calculate $K_{s,2}$ and $K_{s,1}$ values of 3.3 mM and 8.3 mM, respectively, using these same parameters, the experimental values of $K_{m,2}$ and $K_{m,1}$ of 0.25

Scheme 6: Mechanism for the pH Dependence of Catalysis by PBP 2x*

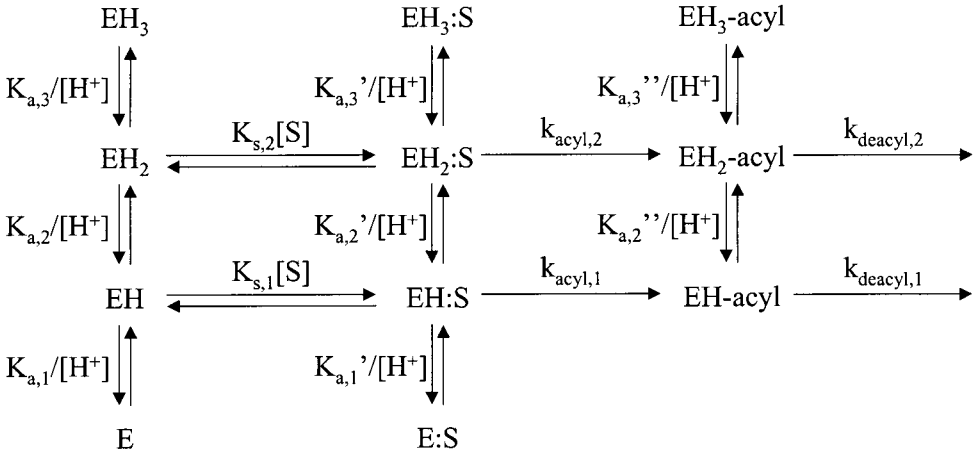

mM and 5.0 mM, respectively, and the general expression of eq 3. This analysis reveals that, in contrast to $K_{m,2}$ and $K_{m,1}$, $K_{s,2}$ and $K_{s,1}$ are similar in magnitude. This discrepancy lies in the 13-fold difference between $K_{m,2}$ and $K_{s,2}$. The depressed value of $K_{m,2}$ is a direct result of the pH-dependent change in rate-limiting step described above. At low pH, deacylation is slow relative to acylation. This kinetic situation allows the acyl-enzyme to accumulate in the steady state, thereby decreasing $K_{m,2}$ relative to the true substrate dissociation constant, $K_{s,2}$.

*Rate Limitation of the Acylation of PBP 2x**. The acylations of PBP 2x* by penicillin G and Bz-(D)Ala-^{S}Gly are complex reactions, each comprising multiple sequential steps, including association, possible conformational isomerizations, and acylation chemistry. We employed two experimental approaches in an attempt to determine the rate-limiting step for these reactions: solvent deuterium isotope effects and temperature dependencies.

Solvent deuterium isotope effects for acylation of serine hydrolases vary widely, from unity to large effects approaching 3 (*10*). Large solvent isotope effects suggest a reaction process that is entirely rate-limited by the chemistry of acylation. In these cases, the solvent isotope effects arises from hydrogen ion fractionation at one or more transition-state protonic bridges of the sort that one encounters in nonenzymic general acid−base catalysis. Small solvent isotope effects suggest one of two mechanisms: (1) partial rate limitation by at least two reaction steps, a chemical step that can generate an isotope effect (e.g., acylation) and a physical reaction step that is isotopically silent (e.g., a conformation change of the enzyme), or (2) rate limitation by chemistry where the large isotope effect that this step generates is offset by solvation effects that occur upon binding of substrate or inhibitor to the enzyme (*13*, *14*). In the present case, we observed a small solvent isotope effect of 1.7 on k_{acyl}/K_s for the PBP 2x*-catalyzed hydrolysis of Bz-(D)Ala-^{S}Gly. With the hope of generating data that would allow us to decide which of the above two mechanistic alternatives can best account for this isotope effect, we performed a proton inventory experiment (Figure 4B).

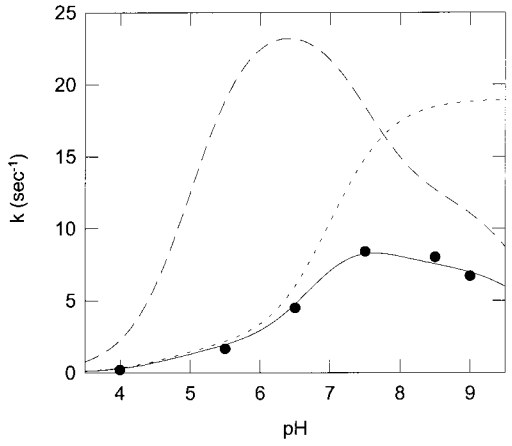

FIGURE 11: Fit of the pH dependence of k_c for the PBP 2x*-catalyzed hydrolysis of Bz-(D)Ala-^{S}Gly to the acyl-enzyme model of Scheme 6. The data points are from Figure 3A and the solid line through them was drawn as described in the text. The dashed and dotted lines are the theoretical pH dependencies for k_{acyl} and k_{deacyl}, respectively.

Proton inventories are experiments in which rate measurements are conducted in mixed isotopic waters and the resultant data are expressed graphically as the dependence of observed rate constant on mole fraction of solvent deuterium. The shape of these curves reflects the number of ground-state and transition-state protonic sites that generate the isotope effect as well as the magnitude of the isotope effect at each of these sites.

The starting point for the analysis of our data, and for proton inventories of serine hydrolase acylation in general, is a modified form of the Gross−Butler equation:

$$k_n = k_0 Z^n \frac{\Pi(1 - n + n\phi_i^{T})}{\Pi(1 - n + n\phi_j^{G})} \qquad (14)$$

where k_n is the observed value of k_{acyl}/K_s at mole fraction of solvent deuterium n, k_0 is the rate constant in pure H_2O (i.e., $n = 0$), Z is a solvation term reflecting the composite isotope effect that is generated by small fractionation factors at many protonic sites, and ϕ_i^{T} and ϕ_j^{G} are the isotopic fractionation factors for the ith and jth proton that is transferred in the transition state and ground state, respectively (*13*, *14*). For reactions of serine hydrolases, ground-state fractionation factors are unity (*10*) and eq 14 simplifies to

$$k_n = k_0 Z^n \Pi(1 - n + n\phi_i^{T}) \qquad (15)$$

If we make the assumption that a single proton is "in flight"

Scheme 7: Expanded Mechanism for the Acylation of PBP 2x*

$$E + S \underset{K_1}{\rightleftharpoons} (E{:}S)_1 \underset{k_{-2}}{\overset{k_2}{\rightleftharpoons}} (E{:}S)_2 \xrightarrow{k_3} E{:}acyl$$

in the transition state, eq 15 can be further simplified to

$$k_n = k_0 Z^n (1 - n + n\phi^T) \quad (16)$$

Best-fit analysis provides the following estimates: $k_0 = 5.1 \pm 0.6$ mM^{-1} s^{-1}, $Z = 1.43 \pm 0.11$, and $\phi^T = 0.401 \pm 0.036$. We see, then, that according to this interpretation, the observed isotope effect of 1.7 results from a chemistry-derived isotope effect of 2.5 ($= 1/\phi^T$) partially offset by a solvation term of 1.4. The chemistry-derived isotope effect is presumably due to general base-catalyzed attack of the active-site serine on substrate carbonyl carbon, while the *Z* term of 1.4 results from the solvent reorganization that occurs upon substrate binding. Similar *Z* terms have been seen observed in other enzyme systems (*13*, *14*).

The other explanation for the dome-shaped proton inventory of Figure 4B involves a mechanism in which two steps partially rate-limit the overall reaction that is governed by k_{acyl}/K_s. This mechanism is illustrated for serine hydrolase acylation in Scheme 7, where an initially formed encounter complex, $(E{\cdot}S)_1$, isomerizes to $(E{\cdot}S)_2$, within which acylation occurs. The rate expression for this mechanism is given by

$$\frac{k_c}{K_m} = \frac{k_{acyl}}{K_s} = \frac{[(k_2 k_3/(k_{-2} + k_3)]}{K_1} \quad (17)$$

Before eq 17 is expanded into an expression for its proton inventory, it is convenient to rearrange it into its reciprocal form:

$$\left(\frac{k_{acyl}}{K_s}\right)^{-1} = \frac{1}{k_2'} + \frac{1}{k_3'} \quad (18)$$

where

$$k_2' = k_2/K_1 \quad (19)$$

and

$$k_3' = \frac{k_3}{K_1(k_{-2}/k_2)} \quad (20)$$

The proton inventory for this system can now be expressed as

$$k_n = Z^n \left\{ \frac{1}{k_2'(1 - n + n\phi^{T2})} + \frac{1}{k_3'(1 - n + n\phi^{T3})} \right\}^{-1} \quad (21)$$

If we assume that the isomerization of $(E{\cdot}S)_1$ to $(E{\cdot}S)_2$ exhibits an isotope effect of unity (i.e., $\phi^{T2} = 1$) and that the *Z* term also approximates 1, then we can determine the following best-fit values for the remaining parameters: $k_2' = 8.6 \pm 1.3$ mM^{-1} s^{-1}, $k_3' = 12.6 \pm 2.5$ mM^{-1} s^{-1}, and $\phi^{T3} = 0.353 \pm 0.052$. Significantly, the line that is generated from eq 21 and these parameters is superimposable on the curved line of Figure 4B.

Table 4: Kinetic and Thermodynamic Parameters for the Enzymatic and Nonenzymatic Hydrolysis of Penicillin G and Bz-(D)Ala-^{S}Gly

penicillin G	Bz-(D)Ala-^{S}Gly	difference[a]
k_E[b] = 83 000 M^{-1} s^{-1}	k_E[b] = 5000 M^{-1} s^{-1}	
$\Delta G^‡$ = 19.1 kcal/mol	$\Delta G^‡$ = 20.9 kcal/mol	$\Delta\Delta G^‡$ = 1.8 kcal/mol
$\Delta H^‡$ = 8.8 kcal/mol	$\Delta H^‡$ = 7.2 kcal/mol	$\Delta\Delta H^‡$ = 1.6 kcal/mol
$T\Delta S^‡$ = 10.3 kcal/mol	$T\Delta S^‡$ = 13.7 kcal/mol	$\Delta(T\Delta S^‡)$ = 3.4 kcal/mol
k_{HO} = 0.1 M^{-1} s^{-1}	k_{HO} = 1.3 M^{-1} s^{-1}	$\Delta\Delta G^‡$ = 1.5 kcal/mol[c]

[a] The difference in thermodynamic parameter is defined as $\Delta\Delta X^‡ = \Delta X^‡_{penicillinG} - \Delta X^‡_{Bz-(D)Ala-SGly}$. [b] k_E are second-order rate constants for acylation of PBP 2x* and correspond to k_{inact}/K_i and k_c/K_m for penicillin G and Bz-(D)Ala-^{S}Gly, respectively. [c] This value was calculated as $RT \ln (k_{HO,Bz(D)Ala-SGly}/k_{HO,penicillinG})$, $T = 298$ K.

We see then that our proton inventory data cannot be uniquely fit to either model for the generation of small solvent isotope effects (see above). Thus, at this time it is unclear how to best explain the small isotope effect for acylation of PBP 2x* by Bz-(D)Ala-^{S}Gly.

The same interpretive considerations obtain for acylation of PBP 2x* by penicillin G, where we observed a solvent isotope effect of 1.25. While the proton inventory for this reaction is linear (data not shown), the data are of insufficient quality to reveal the subtle curvature that would be present in case of a complex reaction mechanism. Again, the data do not allow us to discriminate between the two mechanistic interpretations.

We had hoped that analysis of the Eyring plots for acylation of PBP 2x* by penicillin G and Bz-(D)Ala-^{S}Gly would shed additional light on reaction mechanism. Eyring plots for both reactions are linear and thus may seem more consistent with a single rate-limiting step since two partially rate-limiting steps might be anticipated to give a curved Eyring plot. However, this need not be the case, especially over the limited temperature range that this enzyme can tolerate.

Reactivity of the Active-Site Serine of PBP 2x toward Acylation.* PBP 2x* is acylated 17 times faster by penicillin G than by the thioester Bz-(D)Ala-^{S}Gly (k_{inact}/K_i = 83 000 M^{-1} s^{-1} vs k_{acyl}/K_s = 5000 M^{-1} s^{-1}, respectively). We would like to understand the energetic origins of this difference as it relates to the inherent reactivity of the active-site serine of PBP 2x*.

Now, the 17-fold rate difference that concerns us here corresponds to a $\Delta\Delta G^‡$ of -1.8 kcal/mol, where $\Delta\Delta G^‡$ is defined as $\Delta G^‡_{penicillinG} - \Delta G^‡_{Bz-(D)Ala-SGly}$ (see Table 4 for a summary of this analysis). This free energy term distributes between the enthalpy and entropy of activation in the following way: $\Delta\Delta H^‡ = 1.6$ kcal/mol and $\Delta(T\Delta S)^‡ = -3.4$ kcal/mol ($T = 298$ K). Interestingly, the enthalpy term, in itself, indicates that the thioester is 14 times more reactive as an acylating agent than is penicillin G. This 14-fold difference in reactivity is essentially identical to the 13-fold difference in reactivity toward alkaline hydrolysis that is observed for Bz-(D)Ala-^{S}Gly and penicillin G.

This analysis suggests that the overall reactivity of penicillin G toward PBP 2x*, and possibly other PBPs, results from an interplay between chemical stability and rotational constraint. Thus, we see that during the acylation of PBP 2x* by penicillin G the inherent chemical stability of penicillin's amide bond, as manifested in the enthalpy of activation, is offset by a favorable entropy term that reflects the rotationally constrained state of penicillin's bicyclic

system, which presumably allows a less energetically demanding entry into the transition state for acylation.

REFERENCES

1. Ghuysen, J.-M. (1991) *Annu. Rev. Microbiol. 45*, 37−67.
2. Ghuysen, J.-M. (1997) *Internat. J. Antimicrob. Agents 8*, 45−60.
3. Goffin, C., and Ghuysen, J.-M. (1998) *Microbiol. Mol. Biol. Rev. 62*, 1079−1093.
4. Kell, C., Sharma, U. K., Dowson, C. G., Town, C., Balganesh, T. S., and Spratt, B. G. (1993) *FEMS Microbiol. Lett. 106*, 171−176.
5. Pares, S., Mouz, N., Petillot, Y., Hakenbeck, R., and Dideberg, O. (1996) *Nat. Struct. Biol. 3*, 284−289.
6. Gordon, E., Mouz, N., Duee, E., and Dideberg, O. (2000) *J. Mol. Biol. 299*, 477−485.
7. Jamin, M., Damblon, C., Miller, S., Hakenbeck, R., and Frere, J.-M. (1993) *Biochem. J. 292*, 735−741.
8. Laible, G., Keck, W., Lurz, R., Mottl, H., Frere, J.-M., Jamin, M., and Hakenbeck, R. (1992) *Eur. J. Biochem. 207*, 1007−1009.
9. Brown, R. S., and Aman, A. (1997) *J. Org. Chem. 62*, 4816−4820.
10. Quinn, D. M., and Sutton, L. D. (1991) in *Enzyme Mechanism from Isotope Effects* (Cook, P. F., Ed.) pp 73−126, CRC Press, Boca Raton, FL.
11. Jencks, W. P. (1969). *Catalysis in Chemistry and Enzymology*, pp 517−523, McGraw-Hill, New York.
12. Fersht, A. (1977) *Enzyme Structure and Mechanism*, pp 172−174, W. H. Freeman and Company, New York.
13. Stein, R. L. (1985) *J. Am. Chem. Soc. 107*, 6039−6042.
14. Stein, R. L., Strimpler, A. M., Hori, H., and Powers, J. C. (1987) *Biochemistry 26*, 1305−1314.

BI011368R